

Improving the thermocline calculation over the global ocean

Emmanuel Romero¹, Leonardo Tenorio-Fernandez², Esther Portela^{3,4}, Jorge Montes-Aréchiga⁵, and Laura Sánchez-Velasco¹

¹Instituto Politécnico Nacional-Centro Interdisciplinario de Ciencias Marinas (IPN-CICIMAR), Departamento de Oceanología, Av. IPN s/n, La Paz, B.C.S., 23096, México

²CONACyT-Instituto Politécnico Nacional-Centro Interdisciplinario de Ciencias Marinas (IPN-CICIMAR), Av. IPN s/n, La Paz, B.C.S., 23096, México

³Institute for Marine and Antarctic Studies, University of Tasmania, Hobart 7001, Australia

⁴Univ. Brest, Laboratoire d'Océanographie Physique et Spatiale, CNRS, IRD, Ifremer, Plouzané, France

⁵Universidad de Guadalajara, Departamento de Física, Gral. Marcelino García Barragán 1421, Olímpica, 44430 Guadalajara, Jal, México

Correspondence: Leonardo Tenorio-Fernandez (ltenoriof@ipn.mx)

Abstract. According to the typical thermal structure of the ocean, the water column can be divided into three layers: the ~~mixing~~ mixed layer, the thermocline and the deep layer. In this study, we provide a new methodology, based on a function adjustment on the temperature profile, to locate the minimum and maximum depths of the ~~thermocline, and therefore its thickness, to separate the water column into layers~~ strongest thermocline. We first validated our methodology by comparing the mixed layer depth obtained with the method proposed here with ~~that of two~~ three other methods from previous studies. Since we found a very good agreement between the ~~three~~ four methods we used the function adjustment to compute the monthly climatologies of the ~~mixed layer depth, the~~ maximum depth of the thermocline ~~and,~~ the thermocline thickness ~~, throughout the~~ and strenght, in the global ocean. We also provide an assessment of the regions of the ocean where our adjustment is valid, ~~and consequently the regions i.e.~~ where the thermal structure of the ocean follows the three-layer structure. However, there are ocean regions where the water column cannot be separated into three layers due to the dynamic processes that alter it ~~and the major contribution of salinity to stratification~~. This assessment highlights the limitations of the existing methods to accurately determine the mixed layer depth and the thermocline depth in oceanic regions that are particularly turbulent as the Southern Ocean and the northern North Atlantic, among others. The method proposed here has shown to be robust and easy to apply, ~~and it can be used in both local and global studies~~.

15 1 Introduction

In most of the ocean, a typical ~~profile of temperature over depth~~ vertical temperature profile shows maximum temperature at the surface, due to solar radiation, and can be divided into three main layers according to the thermal structure of the ocean: (i) the mixed layer, where the turbulence generated by atmospheric processes homogenizes the temperature and distributes heat throughout the layer; (ii) the thermocline, the layer with the strongest stratification, that separates the upper mixed layer from
20 the deep layer of the ocean; and (iii) the deep layer, where the temperature is practically invariant over time and relatively

constant from the lower thermocline to the seafloor. This three-layer structure is similar to the fundamental vertical density structure of the world ocean (Sallée et al., 2021), where the central layer is the pycnocline.

In most of the ocean, the temperature exerts the main control on the density of the water column. ~~The exceptions are the polar regions~~ Exceptions to this are mainly found in polar regions, where temperature is very low ~~and~~ and the seawater density is mostly determined by salinity (de Boyer Montégut et al., 2004; Yamaguchi and Suga, 2019; Sallée et al., 2021) ~~and in the so-called Barrier Layer (BL) regions (Lorbacher et al., 2006). The latter, are regions where the mixed layer depth (MLD) is determined by a halocline. In these regions, the MLD based on temperature (the isothermal layer) is deeper than MLD based on density profiles (the isopycnal layer). In the opposite case, when the isothermal layer is shallower than the MLD, the vertical compensation between salinity and temperature causes compensated layers (CL) located below the MLD (de Boyer Montégut et al., 2004).~~

The thermocline is the ocean layer where the temperature changes sharply with depth ~~relative as compared~~ to the upper and lower layers (Fiedler, 2010). Consequently, the thermocline depth is often defined as the depth of the maximum vertical temperature gradient. The characteristics and ~~depths depth~~ of this layer vary ~~latitudinally and longitudinally (coast-ocean gradients). At spatially. In~~ low latitudes, ~~the due to~~ relatively higher temperatures in the upper water column ~~result in strongly stratified thermoclines~~, the stratification is high and permanent thermoclines are relatively strong and thin. In contrast, at high latitudes, where there is generally little difference between the surface and deep layer temperature, the thermocline is ~~weak generally weaker and deeper~~ (Webb, 2021). The strengthening of the upper thermocline in mid-latitudes during summer, when net heat flux at the surface is positive and wind mixing is low, is known as the seasonal thermocline (Sprintall and Cronin, 2001). ~~In contrast, in tropical and polar regions the seasonal changes are weak.~~ Due to cooling, wind-driven mixing, and a well-stratified thermocline, the mixed layer is deeper in winter (Sprintall and Cronin, 2001). In tropical and polar regions the seasonal changes are weak.

~~The mixed layer depth (MLD)~~, Other classifications of the thermocline have been proposed from a machine learning approach. For instance Jiang et al. (2017) classify the thermocline due to its form as positive, inverse and mixed thermoclines as well as multi-thermoclines. The forms that originate this classification could be related to the temperature inversions that occur at the base of the BL and in the polar regions (de Boyer Montégut et al., 2004; Dong et al., 2008) and by the double-diffusive staircase stratification events (Timmermans et al., 2008; Toole et al., 2011).

The MLD (which is also the top of the thermocline, thermocline depth) as well as the maximum thermocline depth (MTD), and thermocline strength (Fiedler, 2010), all play a key role in determining the vertical distribution of many physical and ecological parameters (Fiedler, 2010). The thermocline is a physical gradient that plays a key role in climate variability and ocean-atmosphere interactions (Chu and Fan, 2019). The thermocline strength affects buoyancy, heat budgets, circulation, and exchange of properties. Its depth is associated with the habitat and abundance of zooplankton organisms (Southward and Barrett, 1983; Ruvalcaba-Aroche et al., 2022) and is also an ecological boundary for the pelagic ~~organism because strong organisms. Strong~~ temperature changes can set habitat distributions and ~~because it the thermocline~~ often corresponds to gradients in nutrients (nutricline), oxygen (oxycline), ~~oxygen~~, or other limiting factors. The thermocline thickness also affects the intensity of the primary production. Particularly at the poles, where the thermocline is weaker, enhanced mixing distributes

nutrients throughout the water column. In contrast, in equatorial and tropical regions, the strong thermocline prevents nutrient-rich water from the deep layer from reaching the surface (Webb, 2021). Observations of tracer concentrations and model simulations suggest a connection between the equatorial thermocline and mid-latitude ventilation regions (Harper, 2000).

60 The strength of the ocean stratification has strong implications for the ventilation of the interior ocean and the injection of traces as oxygen and carbon (Sallée et al., 2012; Portela et al., 2020). Therefore, the knowledge and monitoring of the depth and strength of the thermocline is particularly relevant in the context of ocean warming and its effects in the pelagic ecosystem. Recent global studies have found an overall increase of the global ocean stratification (Li et al., 2020) as well as important regional variability in the global pycnocline trend over the past decades (Sallée et al., 2021). For instance, the thickness of the equatorial and tropical thermocline is enhanced under ocean warming, because the surface layer warms more and faster than
65 the lower layers (Yang and Wang, 2009).

Previous regional studies have identified a shallowing and strengthening ~~of the~~ thermocline in the western Pacific Ocean (Vecchi and Soden, 2007) and in the equatorial Pacific (Zelle et al., 2004). Additionally, modeling studies have suggested that important changes in the Pacific Ocean, such as rising sea levels and temperatures, affect the structure of the thermocline from the subtropics to the tropics (Landerer et al., 2007; Overland and Wang, 2007). These changes in thermocline in the
70 western tropical Pacific are considered to influence the properties of ENSO (Luo et al., 2009), which has strong climatic and socio-economical consequences at basin scale, because the organisms change their distribution and abundance.

Different methodologies have been proposed to locate the maximum depth of the mixed layer (~~e.g., de Boyer Montégut et al., 2004; Holte~~ (e.g., de Boyer Montégut et al., 2004; Lorbacher et al., 2006; de Boyer Montégut et al., 2007; Holte and Talley, 2009) and the strength and trends of the ocean stratification (Yamaguchi and Suga, 2019; Li et al., 2020; Sallée et al., 2021). However,
75 little efforts have been dedicated to identify and map the MTD on a global scale. This depth can be delimited empirically by locating the rapid temperature change in the profile, other studies are based in, for instance, calculating the thermocline gradient using the exponential leap-forward gradient method (Chu and Fan, 2017), the maximum curvature point method (Jiang et al., 2016), or using a matrix to calculate the temperature strength of each point and filtering those points that meet the thermocline standard ($> 0.2^{\circ}C/m$) (Jiang et al., 2017). Additionally, Fiedler (2010) has compared different methods to estimate the mixed
80 layer depth, thermocline depth, and thermocline strength. In his study, the method that gave the best results was the Variable Representative Isotherm (VRI). This method locates the thermocline from the base of the mixed layer to the depth at which temperature has dropped halfway toward the deep-water temperature at 400 m (Fiedler, 2010). Despite few studies applying the above methods to particular regions of the ocean, to the best of our knowledge, there are no studies addressing the MTD on a global scale. The methodologies mentioned above to locate the MLD use the data from the profilers of the Argo program. Argo
85 is an international program that measures the ocean water column using a fleet of autonomous profilers, which ~~are capable of measuring pressure, temperature, salinity, and biogeochemical parameters (Argo, 2022a)~~. These profilers move along ocean currents and measure the water column by making profiles from a depth of two kilometers to the surface (Argo, 2022a).

This paper proposes a simple and efficient methodology to locate the minimum and maximum depth of the thermocline and its thickness, making an adjustment of the sigmoid function to the temperature profiles. Locating these depths helps to conduct

90 research on thermocline-related ocean warming and through the proposed methodology, it will be possible to conduct local and global studies on changes in ocean thermal structure through time and space.

2 Data collection

For all the diagnostics carried out in this study we used the Argo dataset. We downloaded the snapshot of January 2022 (Argo, 2022b) and we used the profiles already evaluated by the delayed mode quality control (DMQC) from January 1998 to 95 December 2021 (more than two million), that have been classified as good or probably good data.

We selected pressure, temperature and salinity profiles from the core Argo floats, which typically sample down to 2000 m. We then transformed the in-situ temperature and practical salinity into conservative temperature (Θ), and absolute salinity (S_A), using the definition of the Thermodynamic Equation of SeaWater 2010 (TEOS-10) (McDougall and Barker, 2011).

3 Methodology

100 Previous studies (e.g., de Boyer Montégut et al., 2004; Holte and Talley, 2009) have proposed different methodologies to calculate the MLD on a global scale. Despite the existence of methods to calculate MTD (such as those compared in the revision study of Fiedler (2010)), these have been evaluated with a limited amount of data, and in relatively small tropical and subtropical areas, therefore excluding profiles of high latitudes. Here we propose to use a new method based on the sigmoid function adjustment in the temperature profile to localize the MTD. Our method takes advantage of the characteristics that this 105 function shares with the typical temperature profiles in most of the ocean: a straight line that represents the homogeneity of the MLD, a diagonal that represents the rapid increase or decrease in temperature with depth (changing the sign of the function) in the thermocline, and a straight line that represents the little variability of the temperature of the deep ocean (Figure 1a1).

To locate the MTD, we ~~first computed the~~ computed the relative contribution of temperature (N_T^2) to the vertical maximum of the buoyancy frequency squared (N^2) ~~to locate the most stratified point of the water column. At this point, where the~~ 110 ~~density gradient is the strongest, we consider that it is inside the pycnocline (McDougall and Barker, 2011), and since density is mainly determined by temperature (except at high latitudes), we assume that this point from the temperature profile. We assume that this point~~ is also inside the thermocline (Fiedler, 2010) within the thermocline, as the most stratified point of the water column given by N^2 is inside the pycnocline (McDougall and Barker, 2011). Schematically, most of the temperature profiles in all latitudes have a shape similar to the sigmoid function (~~Equation 1~~) s-shape, ~~for this study we used the logistic function shown in Equation 1, where a is the steepness of the curve and b is the value of the midpoint of the function also known as the inflection point.~~ 115 function shown in Equation 1, where a is the steepness of the curve and b is the value of the midpoint of the function also known as the inflection point.

$$f(x) = \frac{1}{1 + e^{-x}} \frac{1}{1 + e^{-a(x-b)}} \quad (1)$$

To perform the function adjustment, we first locate the ~~most stratified point in the center of the sigmoid function. To this end, greatest absolute value of N_T^2 and~~ we take the temperature profile from the surface to ~~the depth of the most stratified point its depth~~ multiplied by two, in this way, we reduce the ~~maximum depth with which we will work. This is needed to place the sigmoid function, which is symmetrical, in the center of the pycnocline, and data from the deep layer, but making sure not to exclude the isothermal layer or the thermocline. The sigmoid function presents central symmetry with respect to its inflection point, from this point, in both directions, the sigmoid presents a diagonal line, a curve and a straight line. Given these characteristics, by fitting the sigmoid function, we seek to~~ fully represent the mixed layer with a straight line. ~~Then, locate the~~ inflection point in the center of the thermocline and consequently represent the thermocline with the diagonal line.

First, we evaluate the direction of the vertical temperature change. ~~To do this, we compare the temperature value near the surface against the deeper one, if the value closest to the surface is greater, the profile decreases with depth, otherwise it increases.~~ If the temperature decreases with depth, the sigmoid function is inverted by multiplying it by -1 , then we normalize the temperature data between 0 and 1 ~~to make the non-linear adjustment of the function.~~

Next, nonlinear least squares is used to fit the function to obtain the optimal values of the parameters a and b . Once these parameters are obtained, it is possible to approximate the temperature values at any depth above the sigmoid. Despite the central symmetry that the sigmoid function presents, the nonlinear fit of least squares allows the fit to place one straight line shorter than the other one (without losing its shape), thus losing the symmetry and placing the inflection point in the center of the thermocline, regardless of whether or not it coincides with the greatest value of N_T^2 . We assess the goodness of the fit with the coefficient of determination (R^2), this coefficient informs on how well the adjusted function approximates the real data, being 1 the best adjustment.

Once the sigmoid has been fitted to the temperature profile, we can determine the MLD and MTD by scrolling through the function. The temperature at a depth of 10 m resulting from the adjustment of the function is taken as a reference and is denormalized, that is, it is transformed again to be represented as a function of depth. The MLD is then determined as the depth where the potential temperature is $0.2^\circ C$ higher (or lower) than the reference temperature at 10 m (de Boyer Montégut et al., 2004). To locate the MTD, we used the same procedure but going upwards in the function, in this case we take the reference temperature where the deep layer should be located and we look for the difference of $0.2^\circ C$ by decreasing the depth through the function. Because the method is based on a single nonlinear function adjustment, we can have a precision of even centimeters. The procedure explained above can be seen in Figure 1 a and can be used through the script developed (Romero et al., 2022). ~~To visualize the profiles of Figure 1 up to 2 000 m depth, see Figure S1 of the Supplementary information.~~

This methodology was applied to each of the DMQC Argo profiles ~~Before we apply our method to locate the MTD, we have validated it and consequently we provide the monthly average of R^2 in a $2^\circ \times 2^\circ$ grid as a proxy to know the regions of the ocean where the proposed methodology is reliable.~~

~~We have validated the method~~ by comparing our results for the MLD with other existing methods. To do so, the MLD of each profile of the data set was calculated in ~~three-four~~ different ways: (i) with the proposed method, (ii) following the methodology of Holte and Talley (2009) and ~~(iii)~~ with the methodology of de Boyer Montégut et al. (2004) ~~(, using both the (iii) density threshold and the (iv) temperature threshold~~ (hereinafter, we will refer to the former ~~two methods as HT03 and B04 three~~

methods as HT09, B04D and B04T respectively). ~~HT03 separately calculate the MLD for HT09 performs an evaluation of several criteria (calculated from temperature, salinity and density and choose the highest MLD value, while B04 separately)~~ to determine the MLD for each profile, while B04D use a threshold of 0.03 kg m^{-3} compared to the reference value at 10 m depth in the density profile ~~to~~ and B04T an absolute difference of 0.2°C compared to the reference value at the same depth but in the temperature profile, to locate the MLD. To compare the ~~three-four~~ methods to compute ~~de~~ the MLD, the ocean was divided in regions following the reference of the Working Group I contribution to the Sixth Assessment Report (AR6-WGI) (Iturbide et al., 2020) of the Intergovernmental Panel on Climate Change (IPCC) and the regional monthly average of the MLD was calculated. Regions with less than 10 averaged values were not taken into account. ~~Finally, the Spearman correlation was calculated between the results of the four methodologies.~~

To carry out our computations we averaged all profiles available for each climatological month in $2^\circ \times 2^\circ$ cells. The choice of the $2^\circ \times 2^\circ$ cells responds to a compromise between keeping reasonable resolution and enough data in each cell for each climatological month. With these data, we then obtained climatologies of the MLD produced by each methodology described above including the one proposed here. ~~Additionally, we provide the monthly average of R^2 in the same grid as a proxy to know the regions of the ocean where the proposed methodology is reliable. We also computed the relative contribution of temperature (N_T^2) and salinity (N_S^2) to the stratification (N^2) at the most stratified point of the water column, to know the regions where the calculation of the thermocline should also coincide with that of the pycnocline~~ Once the calculation of the MLD was validated, the monthly climatologies of the MTD, the thickness and the strength of the thermocline were obtained. The thermocline strength was calculated using the thermocline strength index (TSI), defined as $\Delta T / \Delta h$, where ΔT and Δh are the differences in temperature and depth, between the MLD and MTD (Yu et al., 2010).

4 Results

~~In order to evaluate the~~ This methodology developed here was applied to each of the DMQC Argo profiles marked as good or probably good data. As a preliminary assessment of the adequacy of the sigmoid function fit, we ~~made~~ performed a first visual exploration of the temperature profiles in different latitudes of the ocean scan of random temperature profiles at different ocean latitudes. Figure 1 shows ~~six temperature profiles~~, illustratively, some examples of different temperature profile adjustment situations with different characteristics and geographical locations, where the MTD and the MLD computed with the method proposed here are indicated.

The temperature profiles shown in Figure 1a, b and f were taken in the northern hemisphere, the profile in Figure 1e in the equator and the a-e were taken from high latitudes to near the equator, while the profiles in Figure 1d and e in the southern hemisphere f-j are located in the North Pacific region during winter months, where thick BL are found (see de Boyer Montégut et al. (2007)). In the profiles from Figure 1a-e the temperature drops in the thermocline as the depth increases, while the profile from profiles in Figure 1f shows and h-j show temperature increase with depth. In both cases our methodology seems to accurately determine the MTD. Profiles in Figure 1e and f show greater variability in their stratification, Figure 1f shows that f and g show the greatest variability in N_T^2 , but the quality of our adjustment differs between them. In

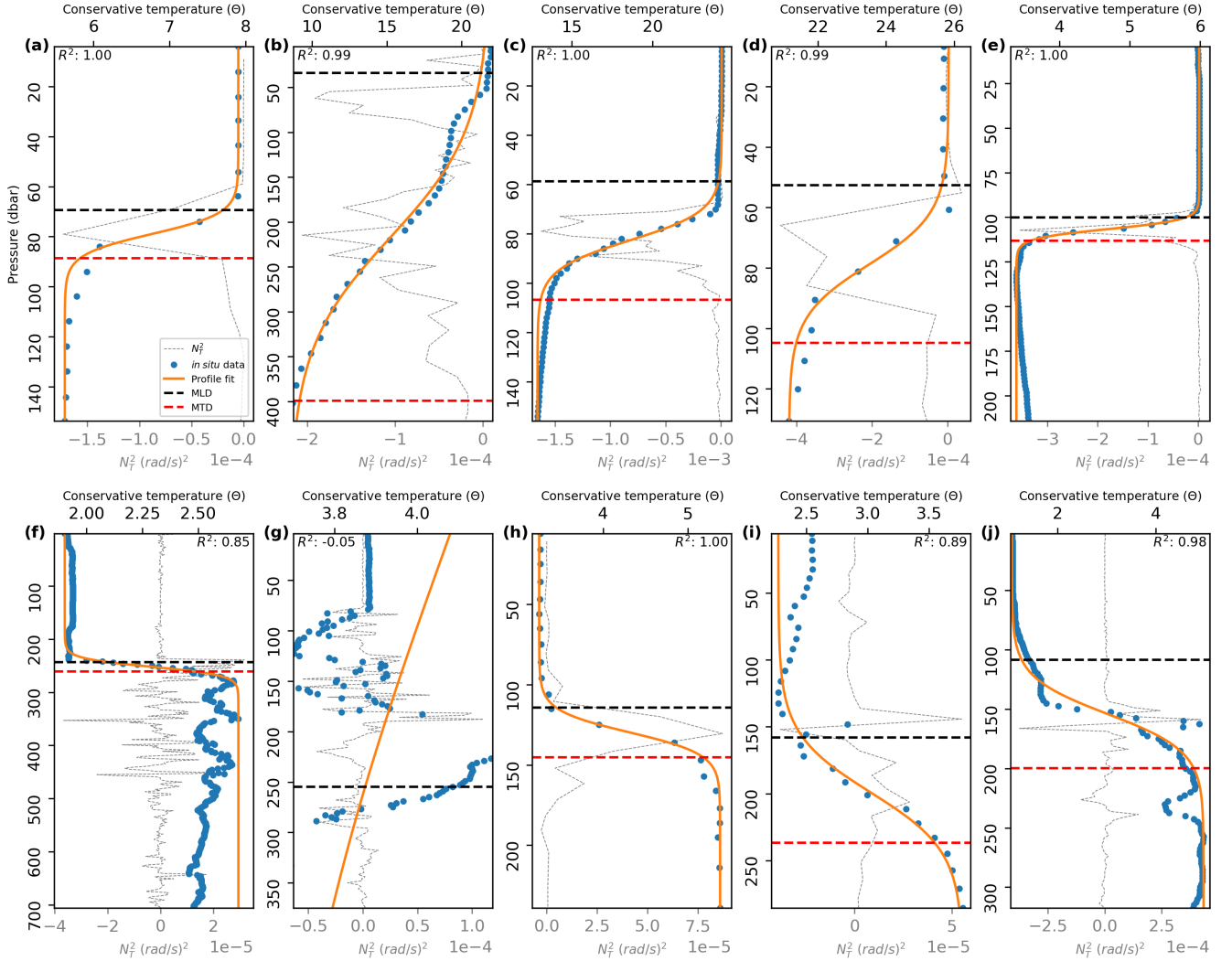


Figure 1. Location of the MTD and the MLD in temperature profiles. (a) 52.95° S and 90.05° W on 01/23/2003. (b) [25.14° S-60.00° S](#) and [93.48° W-116.86° W](#) on 08/12/2015. (c) 25.13° S and 93.47° W on 01/12/2013. (d) [55.42° S](#) and [162.63° W](#) on 08/12/2020. (e) 1.90° S and 126.07° W on 05/08/25/2013. (f) [63.23° N](#) and [54.20° W](#) on 02/08/2010. (g) 20.02° N and [41.15° W-41.14° W](#) on 12/15/2015. (h) [56.07° N](#) and [174.91° W](#) on 02/20/2014. (i) 49.00° N and [174.70° W-174.69° W](#) on 12/13/2017. (j) [60.00° S-61.84° N](#) and [116.86° W-54.27° W](#) on 08/02/12/01/2015-2016. Goodness of fit is shown at the top of each profile with R^2

[panel f](#), despite the high variability in the deep layer, the methodology correctly determines the MLD and MTD. **In all cases R^2 approaches to 1.** Both, the visual examination and the values of R^2 , indicate that our methodology correctly locates the MTD and the MLD at different latitudes.

4.1 Validation of the method: MLD calculation

190 ~~To make the~~ However, in panel g, high variability occurs from the end of the isothermal layer, and our methodology cannot
~~perform the~~ adjustment of the sigmoid function, the most stratified point of the water column is used as the central point of the
adjustment. Figure ?? illustrates the regions of the ocean where salinity (red colors) or temperature (blue colors) dominate the
stratification. This has to be taken into account when interpreting the results of our adjustment, which bases on the temperature
as the main control on density and stratification. Although the N^2 computation is based on density, the stratification of the
195 most stratified point of the water column of most of the ocean is dominated by the temperature, while salinity dominates south
of $60^\circ S$, north of $45^\circ N$ in the Pacific Ocean, in the Labrador Sea and north of $60^\circ N$ in the Atlantic Ocean. Salinity also
dominates the stratification in very localized regions of the tropical ocean such as the Caribbean Sea and the Bay of Bengal,
due to freshwater supply from river runoff, precipitation (Gévaudan et al., 2021), strong rainfall and major river discharge
(Li et al., 2017). In these salinity-dominated regions, the water column does not follow the typical thermal three-layer structure,
200 so our method is not optimal.

Averaged relative contribution of temperature and salinity at the most stratified point of the ocean water column.

In addition to identifying the regions where our method function correctly. In the same way, the B04T, D_σ and VRI methods
failed to correctly locate the MLD and the thermocline (as shown in Figure S1). To illustrate the precision of our method and
to identify regions where it should be applied with caution due to the minor role of temperature in setting the stratification of
205 the water column, we provide another proxy of the goodness of our adjustment. To illustrate the accuracy of our method, to fit
the sigmoid function to variability of the temperature profiles, we provide a map of the monthly average of R^2 (Figure 2).

In general terms, the adjustment of the sigmoid function is very good (with $R^2 \geq 0.9$) in low and mid latitudes. However, the
cells with red and gray colors should be taken with caution. These present $R^2 < 0.3$ and < 0.7 respectively, which indicates
that the adjustment of the sigmoid function was poor or not optimal. The worst adjustments correspond to the core of the
210 Antarctic Circumpolar Current in the Southern Ocean, the North Pacific and the Western North Atlantic. These are regions
where the stratification of the water column is dominated by salinity (Figure ??), there are temperature inversions and/or with
present strong currents and associated turbulent dynamics. In general terms, in the regions where the adjustment was worse, it
was less good in winter months.

Due to the results of the preliminary evaluation, which showed that both the visual examination (not shown) and the values
215 of R^2 indicate that our methodology correctly locates the MTD and the MLD at different latitudes. After this first step, we
carried out the validation against other methodologies.

4.1 Atlas of the mixed layer depth

The monthly climatology of the MLD computed with the proposed method (Figure 3) reproduces well the spatial patterns and
the seasonal variability of the mixed layer as shown in previous studies (e.g., de Boyer Montégut et al., 2004; Holte et al., 2017).
220 It captures the regions with the deepest (northern North Atlantic and Southern Ocean) and the shallowest values (tropical and
subtropical areas of both hemispheres) and their magnitudes.

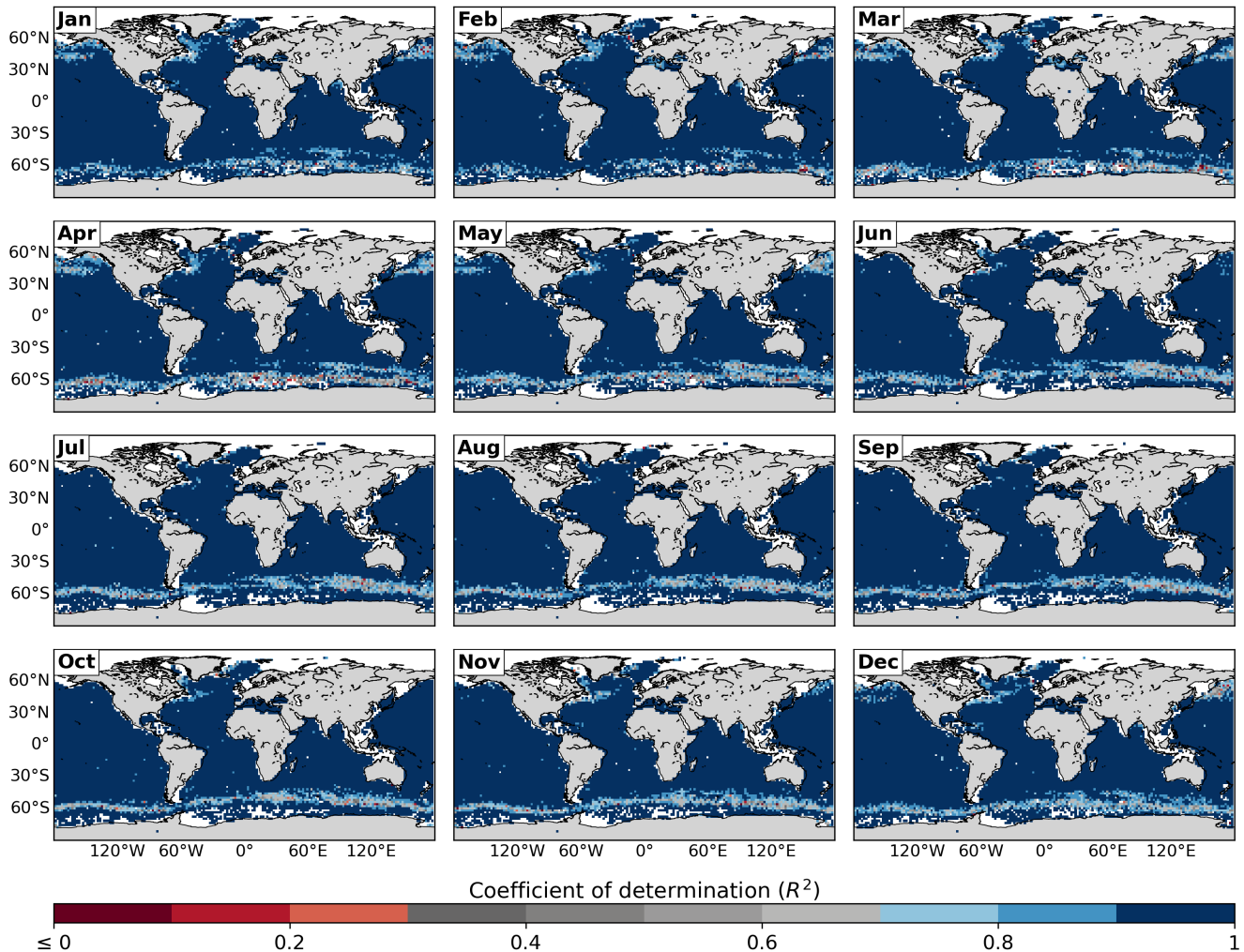


Figure 2. Monthly average of R^2 .

The MLD shows strong seasonality as well as hemispheric asymmetry, mainly in the subtropical and subpolar regions. In the northern hemisphere, in summer months, the mixed layer is generally shallower than 50 m; while in late winter, it reaches climatological mean values over 1000 m in some regions of the North Atlantic basin such as the Labrador Sea, the Nordic Seas. In the Southern hemisphere, the MLD is generally deeper than in the northern hemisphere, and it is dominated by the signal of the Antarctic Circumpolar Current. The mixed layer in this region varies between 75-100 m depth in summer and around 500 m depth in winter, mainly in the Indian and Pacific basins. In tropical and subtropical latitudes, the MLD is generally very shallow, varying below 15 m in summer up to 150 m depth in winter.

In general terms, our climatology agrees with those of Holte et al. (2017), de Boyer Montégut et al. (2004), HT09 and B04 (Figure S1, B04D and B04T (Figure S2-S5 in the Supplementary information), but there are some differences. For

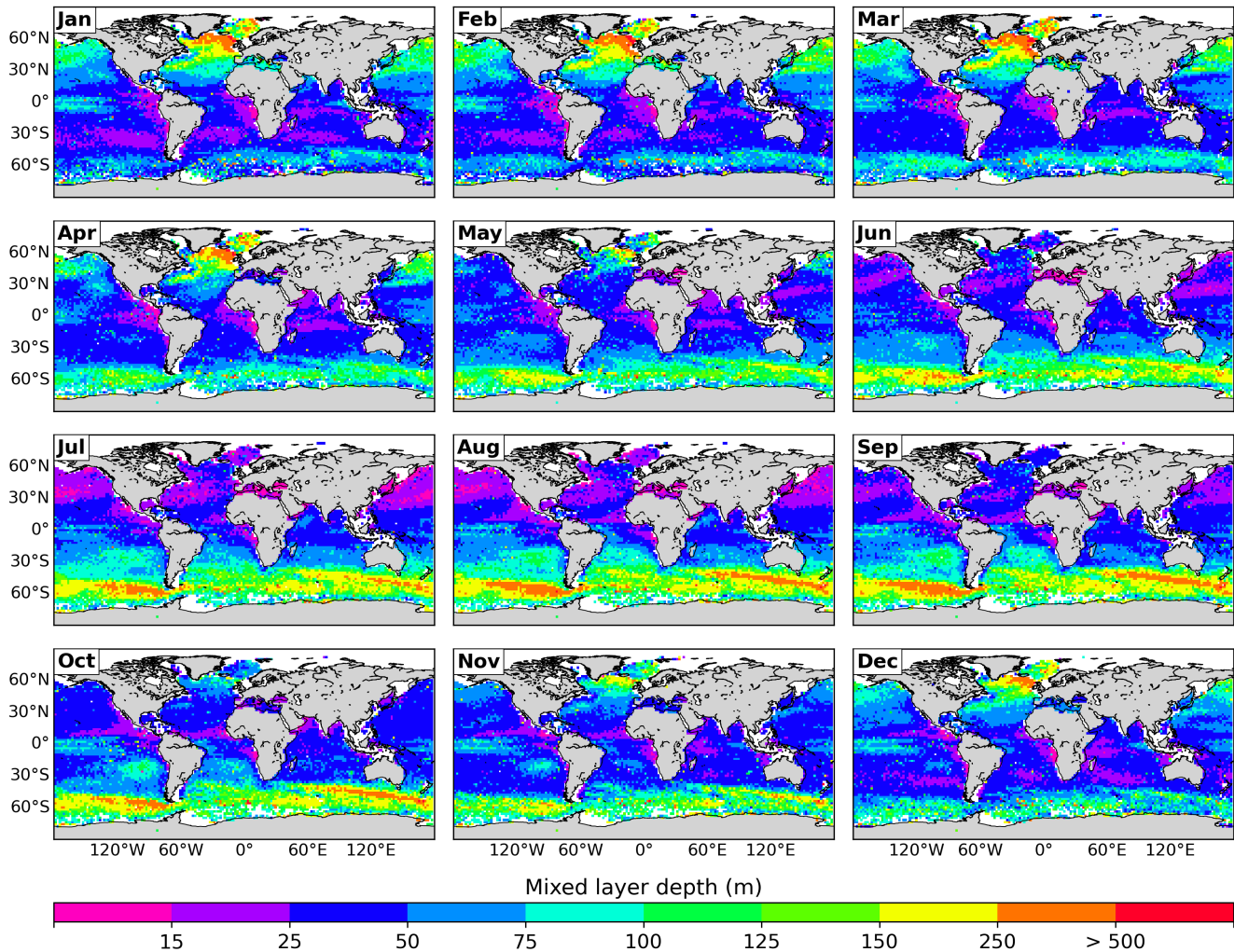


Figure 3. Climatology of the MLD estimated from individual profiles.

instance, Figure S1 shows how B04 generally overestimates the MLD and has the greatest differences (above 25%) compared to our method and HT09 (Figure S2) shows no net underestimation or overestimation and the relative difference between the two methods is less than 25% over most of the ocean. The HT09 method gives slightly shallower mixed layers than our method in subpolar latitudes, while it overestimates the MLD and deeper in tropical and subtropical regions. However, the comparison between our method and B04D and HT09 shows no net underestimation or overestimation and the relative difference between both methods is less than 25% in most of the ocean. B04D generally overestimate the MLD with respect to our method (Figures S2 and S3). B04D has the greatest differences (above 50%) compared to our method, especially in the northern hemisphere from July to September, while B04T presents its greatest differences in tropical and subtropical latitudes throughout the year. To make a more quantitative comparison, the MLDs

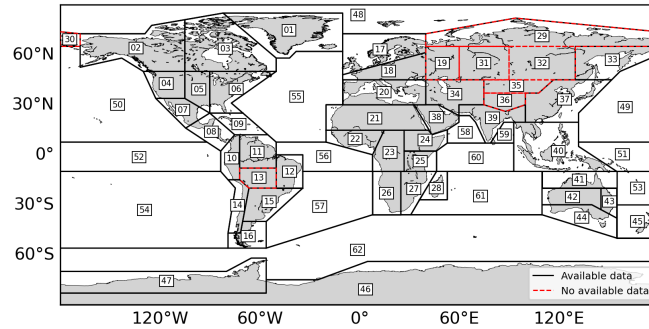


Figure 4. Reference regions of AR6-WGI. The regions used for comparison are those delimited in black.

240 computed with the three-four different methods were averaged within the reference regions of AR6-WGI as described in the methods section, as these were designed for regional synthesis (Figure 4).

The red-delimited regions are fully continental regions and were not used for our analysis. The regions with less than 10 averaged values were also excluded. The averages of the MLD computed with each method in each region were plotted for a representative month of each season (Figure 5).

245 The MLD shows good agreement between the three-four methods in most regions. In general terms, the method proposed here is in better agreement with HT09 and B04T, being B04D, being B04, the one that exhibits the greatest differences. In February and May, the B04-B04D method seems to overestimate the MLD in the regions of Northeast North-America (region and the Arctic-Ocean (regions 03) and North Europe (region 17) (and 48, Figure 5a and bd). These are polar regions containing semi enclosed seas in the Northern Hemisphere and mostly in the Arctic-Ocean (region 48). It is likely that these regions exhibit

250 particular dynamics that complicate the detection of the MLD with a global threshold based method. One possible explanation is that coastal regions generally are worse sampled, but also, that the computation of the MLD can be complicated by a number of coastal processes such as river discharges or shallow bathymetry among others. Moreover, the traditional delta density criterion of 0.03kgm^{-3} has been suggested to underestimate the MLD in polar regions, as demonstrated in the study by Peralta-Ferriz and Woodgate (2015), where it was found that a better criterion for these regions is 0.1kgm^{-3} . Interestingly,

255 the agreement between the three-four methods is also good in the regions where our adjustment was not considered to be good ($R^2 < 0.7$, Figure 2) and in those where salinity dominates the stratification such as region 62 (Figure ??). In other complicated region as the one around Greenland (region 01) there are some differences between the three-four methods, but the one proposed here either agrees completely with one of the other two (B04 in May and November and with B04T in February and HT09 in August) or gives a MLD value that is intermediate regarding the other two, and gives an intermediate MLD value with

260 respect to two other methods (as in February). This May and November. The Spearman correlation between the results was calculated (Figure S5), and showed high correlation between the results of all the methodologies, with the results of HT09 and B04T being the most correlated (0.98), followed by the proposed method and B04T (0.95). Finally, all the correlations between B04D and the rest of the methodologies showed values close to 0.90.

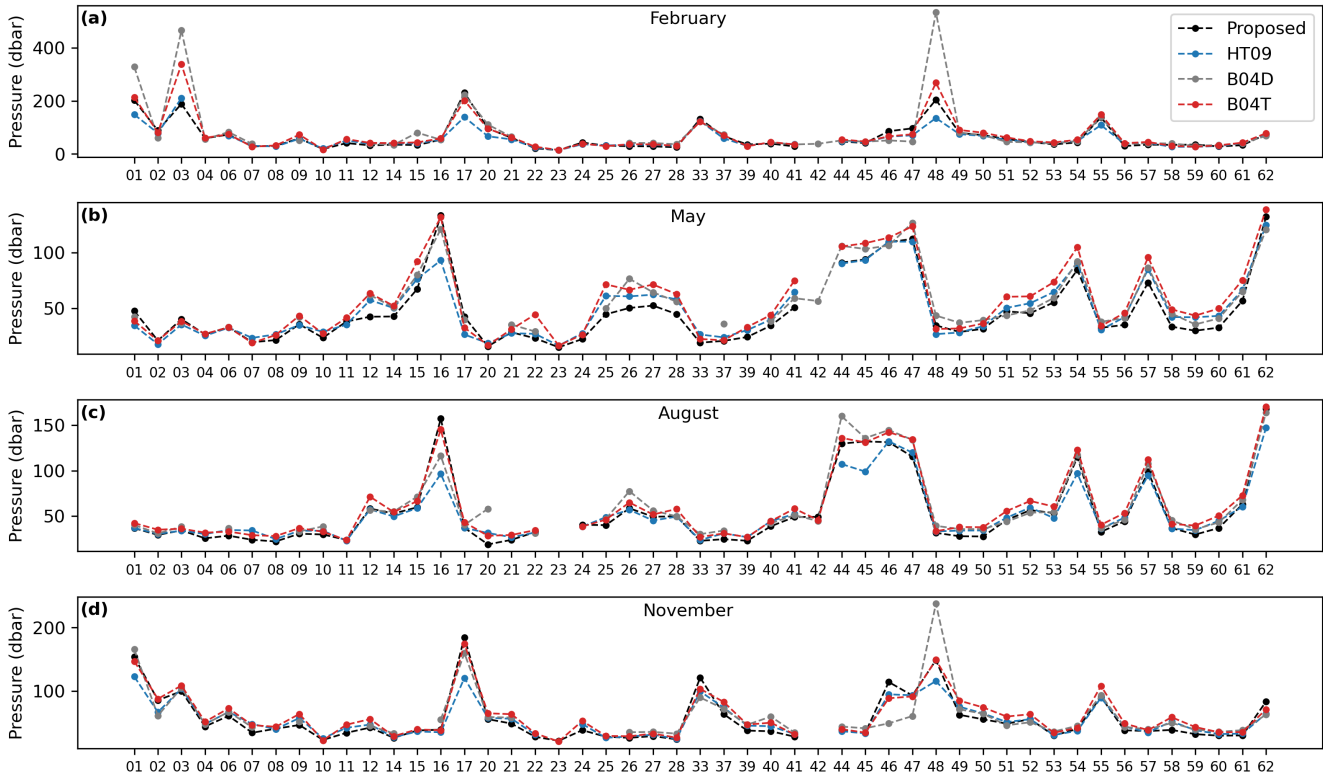


Figure 5. Comparison of methodologies to locate the MLD in (a) February, (b) May, (c) August and (d) November.

265 [All this](#) suggests that although our method is not perfect in ~~these highly dynamical or salinity-dominated~~ [highly dynamical](#) regions, it gives results that compare well with other broadly used methods [to detect the isothermal layer and the MLD, even in salinity-dominated regions](#). Moreover, this highlights the possible deficiency of all existing methods in detecting the MLD in these regions.

4.2 Climatology of the maximum thermocline depth~~and~~, thickness [and strength](#)

Once the proposed methodology is validated with the calculation of the MLD, we computed the monthly climatology of the 270 MTD (Figure 6).

As expected, the shape of the MTD follows that of the MLD but the hemispheric asymmetry is not that evident. The subtropical and subpolar regions of the North Atlantic as well as the Southern Ocean exhibit the deepest thermoclines of the ocean. Similarly to the MLD, the deepest thermoclines are found in late winter: March-April in the Northern Hemisphere and September-October in the Southern Ocean. In the northern hemisphere, during the summer the MTD is generally no deeper than 275 100 m; while in winter, it reaches depths greater than 1000 m in the same regions where the MLD reaches its maximum values

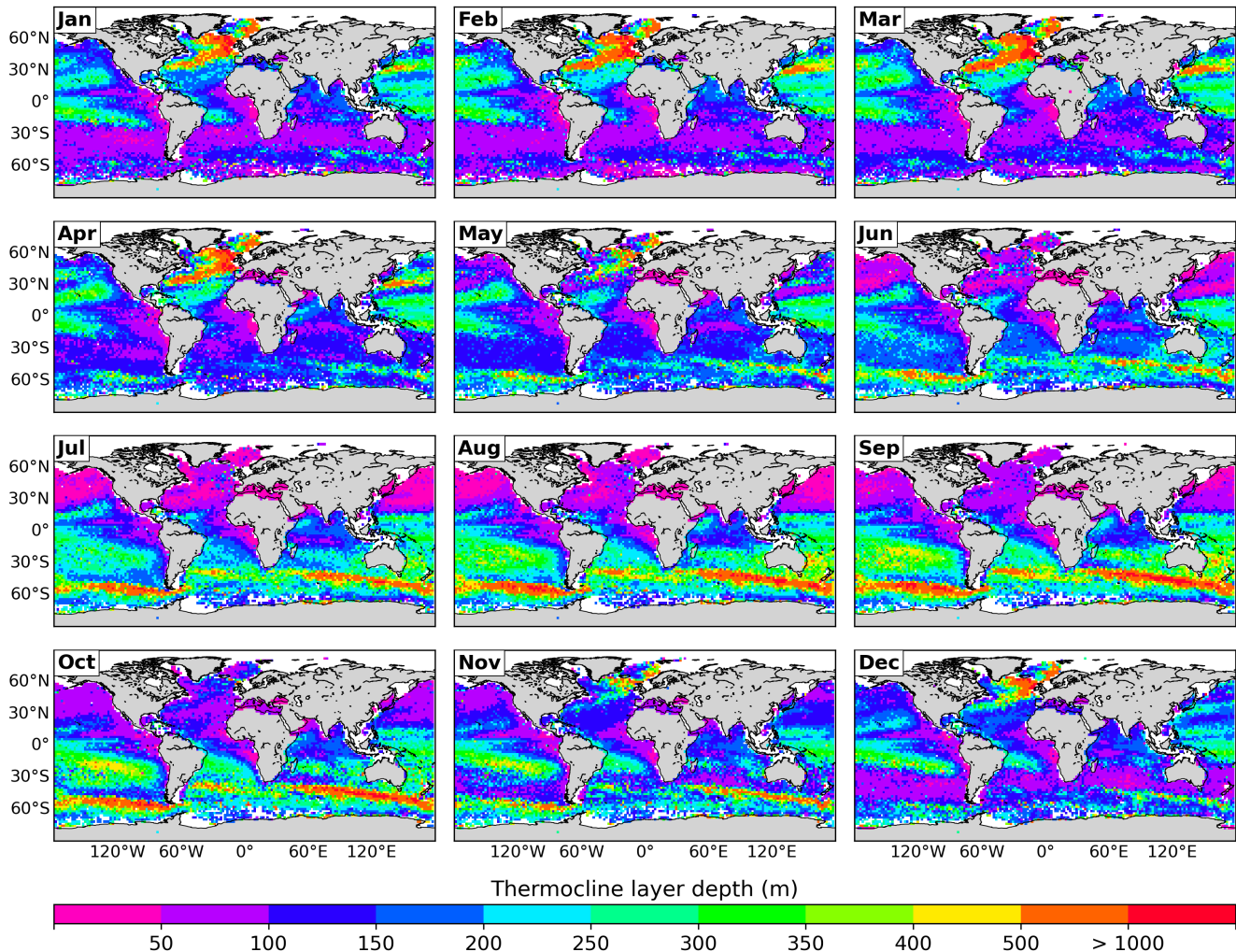


Figure 6. Climatology of the MTD estimated from individual profiles. Shaded cells are those where salinity has a greater contribution to the most stratified point.

(Figure 3), extending to the Gulf Stream in winter and spring months. In the southern hemisphere, the mean climatological MTD values for the summer and winter months are is similar to those of the opposite hemisphere.

This climatology shows the same pattern of greater depths. As in the case of the MLD, MLDs are relatively deep in the Antarctic circumpolar current signal that the MLD climatology shows. During the Circumpolar Current in the Southern Ocean, During winter and spring months, the MTD reaches values deeper than 500 m in the core of the Antarctic Circumpolar Current in the Southern Ocean (in its core, reaching more than 1000 m in localized areas). The deeper thermoclines in the Southern Ocean, in winter, coincide with the seasonality of the zonal band where the inertial horizontal kinetic energy in the

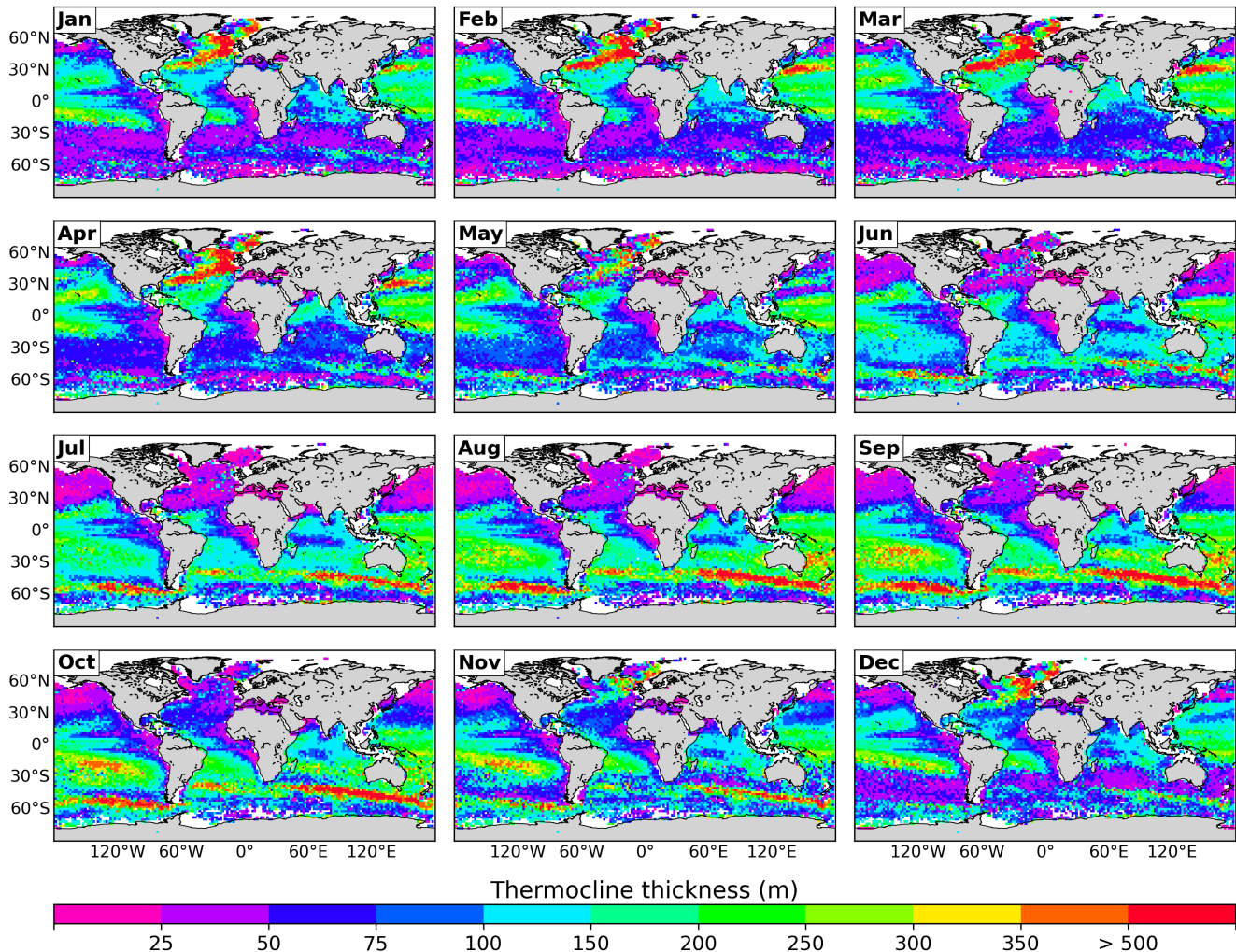


Figure 7. Climatology of the thermocline thickness estimated from individual profiles. ~~Shaded cells are those where salinity has a greater contribution to the most stratified point.~~

mixed layer is larger (Flexas et al., 2019). This energy is injected by the relatively strong winds during ~~these seasons~~ this season, which is also related to the relatively deep MLD (as shown in Figure 3 ~~and therefore of the thermocline~~).

285 During summer, the MTD rarely exceeds 50 m depth in the Northern and 75 m in the Southern Hemisphere. In these same regions, the climatologies of the thermocline thickness (Figure 7) presented mainly values below 50m, ~~which suggests that in the regions where the depths of the MLD and the MTD are very shallow, the thickness of the thermocline is reduced~~ 50 m.

The thermocline thickness follows a similar pattern ~~than as~~ as the MLD and the MTD. In the same ~~way as the MLD and the MDT~~ (Figures 3 and 6 respectively), the climatology of the thermocline thickness (Figure 7) presents a marked seasonality
 290 in subtropical and subpolar latitudes. ~~The thickest thermoclines~~ As expected, the thickest thermoclines (> 500 m) are found

in late winter and in the regions of lower stratification: March-April in the North Atlantic basin and September-October in the Southern Ocean, particularly in the region dominated by the Antarctic Circumpolar Current. Away from these regions, the seasonal variability of the thermocline thickness is low in tropical regions where it varies between 150 and 250 m depending on the region. The thinnest thermoclines are observed in summer in subtropical/subpolar latitudes of both hemispheres (July ~~-August~~ July-August in the Northern Hemisphere and January-February in the Southern Hemisphere).

~~The thermocline thickness follows a similar pattern as the MLD and the MTD. In the same way~~ Finally, the climatology of the thermocline ~~thickness (Figure 7) presents a marked~~ strength (Figure 8) maintains the seasonality in subtropical and subpolar latitudes. ~~As expected, the thickest thermoclines (> 500 m) are found in the regions and periods of lower stratification (i.e., in late winter), March-April in the North Atlantic basin and September-October in the Southern Ocean, particularly in the region~~ dominated by the Antarctic Circumpolar Current. Away from these regions, in tropical latitudes, the seasonal variability of the thermocline thickness is lower, it varies between 150 and 250 m depending on the region. Similarly, the thinnest thermoclines are observed in the most stratified regions, particularly during summer in subtropical/subpolar latitudes of both hemispheres (July-August in the Northern Hemisphere and January-February in the Southern Hemisphere ~~seen previously with a~~ [TSI < 0.1]. On the other hand, the Tropical Eastern Pacific and Tropical Eastern Atlantic have TSI > 0.1 throughout the year, as do the North Pacific and North Atlantic, but from June-November. The Black Sea shows the highest values of TSI (> 1), while the lowest values (< -0.1) are scattered in subpolar regions and in the discharge region of the Ganges-Brahmaputra rivers (December-February).

5 Discussion

In this study we have proposed a new method to locate the ~~thermocline~~ strongest thermocline that lies just below the MLD of the water column. This method is based on the adjustment of a ~~symmetric sigmoid function~~ sigmoid function (in this case the logistic function) that relies on the principle that the thermal structure of the ocean consists of three main layers: the ~~mixing~~ mixed layer, the thermocline and the deep layer of the ocean. Although not all temperature profiles have the ~~shape-s-shape~~ mentioned above throughout the ocean, the proposed method ~~relies on the maximum stratification found within the thermocline and the symmetry of~~ is based on the absolute maximum point of N_T^2 and the nonlinear least squares to fit the sigmoid function, to place the diagonal line of the function in the thermocline. Since the most stratified point of the temperature profile is used to place the sigmoid, the method locates the strongest thermocline which in most cases will coincide with the seasonal one.

The proposed method, due to the shape of a typical temperature profile in the ocean, also allows us to determine the MLD and, therefore, we were able to validate it. The climatology of the MLD generated in our study (Figure 3), is in good agreement with those provided by de Boyer Montégut et al. (2004) and Holte et al. (2017). ~~de Boyer Montégut et al. (2004) used a threshold of 0.03 kg m^{-3} to determine MLD, while Holte et al. (2017) used their two linear function fitting methodology proposed in Holte and Talley (2009). The three methods~~ The four methods compared in this study (based on temperature and density thresholds), reproduce the magnitude, the spatial variability and the seasonal cycle of the MLD throughout the global ocean in a similar and consistent way for most of the ocean regions. This is because most of the ocean the stratification is dominated

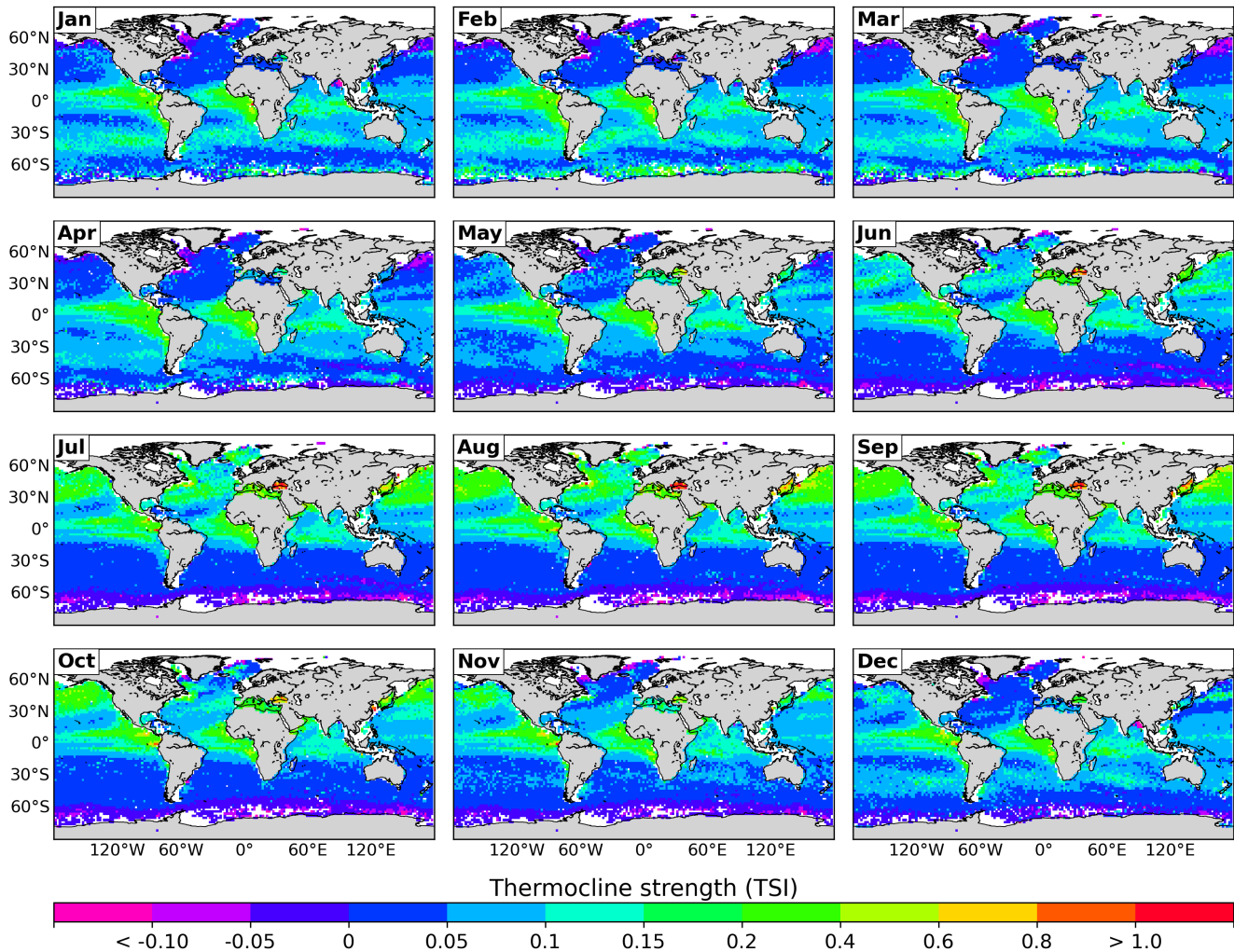


Figure 8. Climatology of the thermocline strength estimated from individual profiles.

by the temperature (de Boyer Montégut et al., 2004). Moreover, in the few regions where all three methods disagreed, the one
 325 proposed here was mostly in line with the results of B04T and HT09, while B04-B04D exhibited extreme MLD values.

~~This can~~ The latter is explained because the proposed method and B04T use the temperature profile and the same threshold
 to calculate the MLD. Moreover, HT09 uses a method that combines different thresholds, including a temperature-based one.
 The coincidences between the proposed method and HT09 can also be partly explained by the fact that both methodologies use
 function adjustments. The study of HT09 bases on the homogeneity of the MLD to perform a linear function adjustment, in
 330 addition to performing another linear function adjustment in the thermocline, while the proposed methodology uses this same
 MLD feature to determine how deep the sigmoid function will be adjusted. The regions with the greatest differences between
 methodologies were found in a small region of the Arctic Ocean and the Labrador Sea (Figure 5a-ba and d). There, the method

of B04 B04D strongly differed from ~~our method and that from HT09. We attribute the overestimation of the B04 method other ones, we attribute this~~ to the fact that staircase stratification have been reported in these areas (Timmermans et al., 2008; Toole et al., 2011) ~~and during the development of this research,~~ defined as BL and CL regions (de Boyer Montégut et al., 2004). ~~Indeed, our preliminary results have shown inverse thermoclines,~~ multi-thermoclines and mix thermoclines (Jiang et al., 2017) ~~have been found~~ in these regions (not shown). In this sense, we have provided some examples of how our method could accurately locate the BL in some cases (Figure S1 of the Supplementary information). In these cases, the MLD calculated by the 0.2°C threshold (B04T) coincides with that calculated with our methodology. Conversely, in other cases, where the isothermal layer was highly variable (Figure S1g and i) our method was unable to locate the thermocline. The BL was also located to these profiles using the D_{σ} and $D_{T-0.2}$ criteria defined in de Boyer Montégut et al. (2007), showing that when the thickness of the BL is of the order of hundreds of meters, the proposed method locates the inverse thermocline produced by the inversion of temperature that is found below the isothermal layer. On the contrary, in thinner BL, our method locates the thermocline below the lower limit of the BL. Sprintall and Tomczak (1992) define the BL as the distance that separates the MLD from the MTD, however, when this BL is thick, the proposed methodology locates the inverse thermoclines that are within this barrier and not those that could be below $D_{T-0.2}$.

All ~~the compared studies~~ previous studies compared here have used Argo data in their climatologies. However, de Boyer Montégut et al. (2004) being an older study had less data, while Holte et al. (2017) used ~~RTQC~~ real-time quality control (RTQC) data in a $1^{\circ}\times 1^{\circ}$ grid (in contrast to the $2^{\circ}\times 2^{\circ}$ grid used by us and de Boyer Montégut et al. (2004)). This smaller-size grid is not optimal to be used with the amount of DMQC data available, ~~as a large number in this snapshot (Argo, 2022b), as about a third~~ of cells would contain less than three values for monthly averages. Using RTQC data would increase the amount of data available for our computations. However, Argo recommends using only DMQC for scientific research, since the RTQC tests are automated and may contain bad data, as explained in the manuals (Argo Data Management Team, 2022) and even using the best quality control flag, as shown in Romero et al. (2021), therefore, using this data could cause the erroneous computation of the MLD and MTD.

Using the density to estimate the MLD usually gives good results, since it depends on temperature and salinity, ~~however,~~ ~~However,~~ the density can show vertical compensation (de Boyer Montégut et al., 2004), ~~therefore, a good alternative to estimate the MLD is to use temperature (Rao et al., 1989). Although the other two below the well-mixed layer (de Boyer Montégut et al., 2004) causing deeper MLDs calculated from density thresholds. Although B04D and HT09 methods use density profiles for the calculation of the MLD, this does not give good results with the methodology proposed in this paper. The adjustment of the sigmoid function bases on the typical shape of the temperature profile. In order to calculate the pycnocline with a similar methodology to the one proposed here, it would be necessary to find another function that better fits the density profile. Yamaguchi and Suga (2019) decomposed density stratification into haline and thermal stratification components, and showed that thermal stratification trends contribute more to density stratification trends since, since despite also being able to be represented in three layers, the 1960s. Only in regions where salinity is significant (e.g., Subarctic North Pacific, Southern Ocean), salinity stratification trends show contributions to density stratification trends. As shown in Figure ??, in more than 77% of the grid cells the N_T^2 contribution to the maximum stratification of the water column, is equal to or greater than 50%.~~

Therefore our method assumes that in these regions, the maximum N^2 is a good approximation of both, the thermocline, and the pycnocline typical density profiles present an inclination along the entire profile, which makes it difficult to fit a conventional sigmoid function. In the polar and some subpolar regions of both hemispheres, where salinity is the major contributor to the density gradient (reddish cells in Figure ??) it dominates the stratification. Consequently, in these regions, In these cases the thermocline and pycnocline might may differ significantly, and our method cannot be used to approximate the pycnocline this is why MLD calculations based on temperature profiles differ considerably from those based on density in these regions.

The calculation of the climatologies of the MTD and the thermocline thickness and thermocline strength were not compared with the calculation of any other method since no method of calculating these parameters was found that works on a global scale. The latter was reproduced here, Helber et al. (2012) mention that the transition layer thickness (TLT) used in their study may encompass the entire thickness of the thermocline, and in fact their TLT climatology presents some coincidences with our climatology of the thermocline thickness (Figure 7). The most notorious coincidences are in the regions of the northeast Pacific Ocean, the northern North Atlantic Ocean and the Antarctic Circumpolar Current in the Southern Ocean, where the thermocline thickness and the TLT show values greater than 350 m in the winter months, in addition to the marked seasonality that both presents in tropical and subtropical regions. Regarding the climatology of the thermocline strength (Figure 8), it was calculated through the TSI, this index indicates the steepness of the thermocline (Duka et al., 2021). The further TSI is from 0, the slope is less steep and therefore the thermocline is stronger. The strongest thermoclines found in the Black Sea are associated with thin thermoclines (15-20 m) between warm surface waters and cold intermediate waters (20 – 8°) (Akpınar et al., 2017) which produce small slopes. Negative values of TSI are caused by inverse thermoclines, these were found mainly in subpolar regions and in the Ganges-Brahmaputra rivers discharge, these regions present TSI close to 0, which means steep slopes and therefore weak thermoclines. The formation of intermediate strength thermoclines (i.e. $0.2 < \text{TSI} < 0.8$) in the North Pacific and North Atlantic coincides mainly with the months (July-September) when there are no BL in these regions (de Boyer Montégut et al., 2007). On the contrary, from January-March when the BL are thicker (de Boyer Montégut et al., 2007), weak thermoclines and regions with inverse thermoclines are shown.

To compare the location of the MTD, the VRI method was applied to the profiles shown in Figure S1 and only gave good results with profiles located in tropical latitudes Fiedler (2010), and only gave good results with profiles those located in tropical latitudes (Figure S2 in the Supplementary information). As shown in Figure S2, away S1, far from the tropics, the calculation of the MLD and MTD with the VRI method does not give good results, in addition to not considering the inverse thermoclines (Figure S2f S1f-j). For these reasons, the relative contribution of temperature and salinity to the most stratified point of the water column and the performance in fitting the sigmoid function were used to validate the method.

Our In different areas of knowledge, R^2 is used as a goodness-of-fit measure for sigmoid functions (e.g., Cao et al., 2019; Bhogal et al., 2019), through this measure, our method showed generally good performance in the adjustment of the sigmoid function to the temperature profiles (expressed by the R^2) with the exception of a few regions: the North Pacific Ocean, the northern North Atlantic Ocean, the Arctic Ocean and the core of the Antarctic Circumpolar Current in the Southern Ocean. While the interpretation of the MLD and the MTD in these regions has to be made with caution, it is noteworthy that the values of R^2 are not a direct indicator of the precision of the method to calculate the MLD and the MTD. Rather, this index shows the goodness of the

sigmoid function fit to the temperature profile. Precisely, in the most problematic regions mentioned above, R^2 is lower than 0.7 in some months (Figure 2). However, the three methods used for the MLD calculation give very similar values (Figure 5) even in these regions. This suggests that it is not a particular shortcoming of our adjustment. Previous studies such as those by Peralta-Ferriz and Woodgate (2015) and [Pellichero et al. \(2017\)](#) have shown the variability in the calculation of the MLD in these regions depending on the methods and thresholds used. This has evidenced that these are complex, highly dynamical regions (i.e., turbulent regions with important eddy activity), where the estimation of the MLD in a reliable way is a complicated task. In this sense, it has been suggested that in the Southern Ocean the MLD calculation is less accurate than in regions at lower latitudes where the water column is strictly temperature stratified (Dong et al., 2008). The low values of R^2 shown in Figure 2 are due to the abrupt changes in temperature in the profiles measured in these regions. These abrupt changes might be related to well known processes taking place in certain regions of the ocean as: (i) double-diffusive staircase stratification in the Arctic (Timmermans et al., 2008; Toole et al., 2011), and (ii) to the temperature inversions due to the influence of salinity that present different vertical structures in the Southern Ocean (Dong et al., 2008).

The results of our adjustment also evidence the regions of the ocean where the water column exhibits a typical vertical thermal structure in three layers and the regions where, due to their dynamics, the structure of the water column cannot be divided in these three layers. The efficiency provided by the proposed method for the calculation of the MLD and the MTD, allows to perform local to global studies. For example, in the context of ocean warming, the differences of these layers could be compared [temporarily over different timescales](#) to analyze the changes of the water column, detecting areas of the ocean where the thermocline has changed its ~~depth or thickness~~, [thickness or strength](#) over time, and therefore to be a parameter of the potential effects on the pelagic ecosystem and socio-economic repercussions.

6 Conclusions

In this study, we present a methodology to locate the minimum and maximum ~~depth of the thermocline and its thickness~~ [depths of the strongest thermocline, its thickness and its strength](#) by adjusting the sigmoid function to the temperature profiles in the global ocean. This methodology can be applied ~~to both global and local studies~~ in those areas of the ocean where the water column can be divided into three layers according to its thermal structure. Our methodology gave good results in its validation against other ~~two three~~ broadly used methodologies in the global ocean. The MLD computed with the ~~three four~~ methods showed a high correlation, even in regions where the coefficient of determination suggested a poor adjustment. This suggests that it is not a particular shortcoming of our method, but rather a general difficulty in determining the limits of the three typical oceanic thermal layers in highly turbulent regions.

Code availability. The methodology presented in this study was developed in Python 3.7 and is licensed under a Creative Commons Attribution 4.0 International License. The source code is available at <https://doi.org/10.5281/zenodo.6985561> (Romero et al., 2022). The latest package version is v1.1.0.

435 *Data availability.* These data were collected and made freely available by the International Argo Program and the national programs that contribute to it (<https://argo.ucsd.edu>, last access: January 2022; <https://www.ocean-ops.org>, last access: January 2022). The Argo Program is part of the Global Ocean Observing System. The data used belongs to the snapshot of January 2022 (Argo, 2022b).

Author contributions. ER developed the methodology described in this work and carried out the analyses. All co-authors contributed to the conceptualization and design of the study, the interpretation of the results, and the preparation of the article.

Competing interests. The authors declare that they have no conflict of interest.

440 *Acknowledgements.* We are grateful to CONACYT for granting scholarship no. 780669 to Emmanuel Romero. We appreciate that these data were collected and made freely available by the International Argo Program and the national programs that contribute to it (<https://argo.ucsd.edu>, last access: January 2022; <https://www.ocean-ops.org>, last access: January 2022). The Argo Program is part of the Global Ocean Observing System. We also thank the Centro Interdisciplinario de Ciencias Marinas (CICIMAR) for their institutional support. We also acknowledge the critical comments from the reviewers.

445 References

- Akpinar, A., Fach, B. A., and Oguz, T.: Observing the subsurface thermal signature of the Black Sea cold intermediate layer with Argo profiling floats, *Deep Sea Research Part I: Oceanographic Research Papers*, 124, 140–152, <https://doi.org/https://doi.org/10.1016/j.dsr.2017.04.002>, 2017.
- Argo: Argo, <https://argo.ucsd.edu/>, 2022a.
- 450 Argo: Argo float data and metadata from Global Data Assembly Centre (Argo GDAC), <https://doi.org/10.17882/42182>, 2022b.
- Argo Data Management Team: Argo user’s manual, <https://doi.org/10.13155/29825>, 2022.
- Bhogal, A. A., Siero, J. C., Fisher, J. A., Froeling, M., Luijten, P., Philippens, M., and Hoogduin, H.: Investigating the non-linearity of the BOLD cerebrovascular reactivity response to targeted hypo/hypercapnia at 7T, *NeuroImage*, 98, 296–305, <https://doi.org/https://doi.org/10.1016/j.neuroimage.2014.05.006>, 2014.
- 455 Cao, L., Shi, P.-J., Li, L., and Chen, G.: A New Flexible Sigmoidal Growth Model, *Symmetry*, 11, <https://doi.org/10.3390/sym11020204>, 2019.
- Chu, P. C. and Fan, C.: Exponential leap-forward gradient scheme for determining the isothermal layer depth from profile data, *Journal of Oceanography*, 73, 503–526, <https://doi.org/10.1007/s10872-017-0418-0>, 2017.
- Chu, P. C. and Fan, C.: Global ocean synoptic thermocline gradient, isothermal-layer depth, and other upper ocean parameters, *Scientific*
- 460 *Data*, 6, 119, <https://doi.org/10.1038/s41597-019-0125-3>, 2019.
- de Boyer Montégut, C., Madec, G., Fischer, A. S., Lazar, A., and Iudicone, D.: Mixed layer depth over the global ocean: An examination of profile data and a profile-based climatology, *Journal of Geophysical Research: Oceans*, 109, <https://doi.org/10.1029/2004JC002378>, 2004.
- de Boyer Montégut, C., Mignot, J., Lazar, A., and Cravatte, S.: Control of salinity on the mixed layer depth in the world ocean: 1. General description, *Journal of Geophysical Research: Oceans*, 112, <https://doi.org/https://doi.org/10.1029/2006JC003953>, 2007.
- 465 Dong, S., Sprintall, J., Gille, S. T., and Talley, L.: Southern Ocean mixed-layer depth from Argo float profiles, *Journal of Geophysical Research: Oceans*, 113, <https://doi.org/10.1029/2006JC004051>, 2008.
- Duka, M. A., Shintani, T., and Yokoyama, K.: Thermal stratification responses of a monomictic reservoir under different seasons and operation schemes, *Science of The Total Environment*, 767, 144 423, <https://doi.org/https://doi.org/10.1016/j.scitotenv.2020.144423>, 2021.
- Fiedler, P. C.: Comparison of objective descriptions of the thermocline, *Limnology and Oceanography: Methods*, 8, 313–325, <https://doi.org/10.4319/lom.2010.8.313>, 2010.
- 470 Flexas, M. M., Thompson, A. F., Torres, H. S., Klein, P., Farrar, J. T., Zhang, H., and Menemenlis, D.: Global Estimates of the Energy Transfer From the Wind to the Ocean, With Emphasis on Near-Inertial Oscillations, *Journal of Geophysical Research: Oceans*, 124, 5723–5746, <https://doi.org/10.1029/2018JC014453>, 2019.
- Gévaudan, M., Jouanno, J., Durand, F., Morvan, G., Renault, L., and Samson, G.: Influence of ocean salinity stratification on the tropical
- 475 *Atlantic Ocean surface*, *Climate Dynamics*, 57, 321–340, <https://doi.org/10.1007/s00382-021-05713-z>, 2021.
- Harper, S.: Thermocline ventilation and pathways of tropical–subtropical water mass exchange, *Tellus A: Dynamic Meteorology and Oceanography*, 52, 330–345, <https://doi.org/10.3402/tellusa.v52i3.12269>, 2000.
- Helber, R. W., Kara, A. B., Richman, J. G., Carnes, M. R., Barron, C. N., Hurlburt, H. E., and Boyer, T.: Temperature versus salinity gradients below the ocean mixed layer, *Journal of Geophysical Research: Oceans*, 117, <https://doi.org/https://doi.org/10.1029/2011JC007382>, 2012.
- 480 Holte, J. and Talley, L.: A New Algorithm for Finding Mixed Layer Depths with Applications to Argo Data and Subantarctic Mode Water Formation, *Journal of Atmospheric and Oceanic Technology*, 26, 1920–1939, <https://doi.org/10.1175/2009JTECHO543.1>, 2009.

- Holte, J., Talley, L. D., Gilson, J., and Roemmich, D.: An Argo mixed layer climatology and database, *Geophysical Research Letters*, 44, 5618–5626, <https://doi.org/10.1002/2017GL073426>, 2017.
- 485 Iturbide, M., Gutiérrez, J. M., Alves, L. M., Bedia, J., Cerezo-Mota, R., Cimadevilla, E., Cofiño, A. S., Luca, A. D., Faria, S. H., Gorodetskaya, I. V., Hauser, M., Herrera, S., Hennessy, K., Hewitt, H. T., Jones, R. G., Krakovska, S., Manzanas, R., Martínez-Castro, D., Narisma, G. T., Nurhati, I. S., Pinto, I., Seneviratne, S. I., van den Hurk, B., and Vera, C. S.: An update of IPCC climate reference regions for subcontinental analysis of climate model data: definition and aggregated datasets, *Earth System Science Data*, 12, 2959–2970, <https://doi.org/10.5194/essd-12-2959-2020>, 2020.
- 490 Jiang, B., Wu, X., and Ding, J.: Comparison of the calculation methods of the thermocline depth of the South China Sea, *Mar. Sci. Bull*, 35, 64–73, 2016.
- Jiang, Y., Gou, Y., Zhang, T., Wang, K., and Hu, C.: A Machine Learning Approach to Argo Data Analysis in a Thermocline, *Sensors*, 17, <https://doi.org/10.3390/s17102225>, 2017.
- Landerer, F. W., Jungclauss, J. H., and Marotzke, J.: Regional Dynamic and Steric Sea Level Change in Response to the IPCC-A1B Scenario, *Journal of Physical Oceanography*, 37, 296–312, <https://doi.org/10.1175/JPO3013.1>, 2007.
- 495 Li, G., Cheng, L., Zhu, J., Trenberth, K. E., Mann, M. E., and Abraham, J. P.: Increasing ocean stratification over the past half-century, *Nature Climate Change*, 10, 1116–1123, <https://doi.org/10.1038/s41558-020-00918-2>, 2020.
- Li, Y., Han, W., Ravichandran, M., Wang, W., Shinoda, T., and Lee, T.: Bay of Bengal salinity stratification and Indian summer monsoon intraseasonal oscillation: 1. Intraseasonal variability and causes, *Journal of Geophysical Research: Oceans*, 122, 4291–4311, <https://doi.org/https://doi.org/10.1002/2017JC012691>, <https://doi.org/10.1002/2017JC012691>, 2017.
- 500 Liu, W. and Saint, D. A.: Validation of a quantitative method for real time PCR kinetics, *Biochemical and Biophysical Research Communications*, 294, 347–353, [https://doi.org/https://doi.org/10.1016/S0006-291X\(02\)00478-3](https://doi.org/https://doi.org/10.1016/S0006-291X(02)00478-3), 2002.
- Lorbacher, K., Dommenges, D., Niiler, P. P., and Köhl, A.: Ocean mixed layer depth: A subsurface proxy of ocean-atmosphere variability, *Journal of Geophysical Research: Oceans*, 111, <https://doi.org/https://doi.org/10.1029/2003JC002157>, 2006.
- Luo, Y., Rothstein, L. M., and Zhang, R.-H.: Response of Pacific subtropical-tropical thermocline water pathways and transports to global warming, *Geophysical Research Letters*, 36, <https://doi.org/10.1029/2008GL036705>, 2009.
- 505 McDougall, T. and Barker, P.: Getting started with TEOS-10 and the Gibbs Seawater (GSW) Oceanographic Toolbox, *SCOR/IAPSO WG127*, 2011.
- Overland, J. E. and Wang, M.: Future climate of the north Pacific Ocean, *Eos, Transactions American Geophysical Union*, 88, 178–182, <https://doi.org/10.1029/2007EO160003>, 2007.
- 510 Pellichero, V., Sallée, J.-B., Schmidtko, S., Roquet, F., and Charrassin, J.-B.: The ocean mixed layer under Southern Ocean sea-ice: Seasonal cycle and forcing, *Journal of Geophysical Research: Oceans*, 122, 1608–1633, <https://doi.org/10.1002/2016JC011970>, 2017.
- Peralta-Ferriz, C. and Woodgate, R. A.: Seasonal and interannual variability of pan-Arctic surface mixed layer properties from 1979 to 2012 from hydrographic data, and the dominance of stratification for multiyear mixed layer depth shoaling, *Progress in Oceanography*, 134, 19–53, <https://doi.org/10.1016/j.pocean.2014.12.005>, 2015.
- 515 Portela, E., Kolodziejczyk, N., Vic, C., and Thierry, V.: Physical Mechanisms Driving Oxygen Subduction in the Global Ocean, *Geophysical Research Letters*, 47, e2020GL089040, <https://doi.org/https://doi.org/10.1029/2020GL089040>, 2020.
- Rao, R. R., Molinari, R. L., and Festa, J. F.: Evolution of the climatological near-surface thermal structure of the tropical Indian Ocean: 1. Description of mean monthly mixed layer depth, and sea surface temperature, surface current, and surface meteorological fields, *Journal of Geophysical Research: Oceans*, 94, 10 801–10 815, <https://doi.org/10.1029/JC094iC08p10801>, 1989.

- 520 Ritz, C. and Spiess, A.-N.: qpcR: an R package for sigmoidal model selection in quantitative real-time polymerase chain reaction analysis, *Bioinformatics*, 24, 1549–1551, <https://doi.org/10.1093/bioinformatics/btn227>, 2008.
- Romero, E., Tenorio-Fernandez, L., Castro, I., and Castro, M.: Filtering method based on cluster analysis to avoid salinity drifts and recover Argo data in less time, *Ocean Science*, 17, 1273–1284, <https://doi.org/10.5194/os-17-1273-2021>, 2021.
- Romero, E., Tenorio-Fernandez, L., Portela, E., Montes-Aréchiga, J., and Sánchez-Velasco, L.: romeroqe/mld-mtd: MLD&MTD, 525 <https://doi.org/10.5281/zenodo.6985561>, 2022.
- Ruvalcaba-Aroche, E. D., Sánchez-Velasco, L., Beier, E., Barton, E. D., Godínez, V. M., Gómez-Gutiérrez, J., and Martínez-Rincón, R. O.: Ommastrephid squid paralarvae potential nursery habitat in the tropical-subtropical convergence off Mexico, *Progress in Oceanography*, 202, 102762, <https://doi.org/10.1016/j.pocean.2022.102762>, 2022.
- Sallée, J.-B., Matear, R. J., Rintoul, S. R., and Lenton, A.: Localized subduction of anthropogenic carbon dioxide in the Southern Hemisphere 530 oceans, *Nature Geoscience*, 5, 579–584, <https://doi.org/10.1038/ngeo1523>, 2012.
- Sallée, J.-B., Pellichero, V., Akhoudas, C., Pauthenet, E., Vignes, L., Schmidtko, S., Garabato, A. N., Sutherland, P., and Kuusela, M.: Summertime increases in upper-ocean stratification and mixed-layer depth, *Nature*, 591, 592–598, <https://doi.org/10.1038/s41586-021-03303-x>, 2021.
- Southward, A. J. and Barrett, R. L.: Observations on the vertical distribution of zooplankton, including post-larval teleosts, off Plymouth in the 535 presence of a thermocline and a chlorophyll-dense layer, *Journal of Plankton Research*, 5, 599–618, <https://doi.org/10.1093/plankt/5.4.599>, 1983.
- Sprintall, J. and Cronin, M. F.: Upper Ocean Vertical Structure, <https://doi.org/10.1006/rwos.2001.0149>, 2001.
- Sprintall, J. and Tomczak, M.: Evidence of the barrier layer in the surface layer of the tropics, *Journal of Geophysical Research: Oceans*, 97, 7305–7316, <https://doi.org/https://doi.org/10.1029/92JC00407>, 1992.
- 540 Timmermans, M.-L., Toole, J., Krishfield, R., and Winsor, P.: Ice-Tethered Profiler observations of the double-diffusive staircase in the Canada Basin thermocline, *Journal of Geophysical Research: Oceans*, 113, <https://doi.org/10.1029/2008JC004829>, 2008.
- Toole, J. M., Krishfield, R. A., Timmermans, M.-L., and Proshutinsky, A.: The ice-tethered profiler: Argo of the Arctic, *Oceanography*, 24, 126–135, <http://www.jstor.org/stable/24861307>, 2011.
- Van der Graaf, P. and Schoemaker, R.: Analysis of asymmetry of agonist concentration–effect curves, *Journal of Pharmacological and 545 Toxicological Methods*, 41, 107–115, [https://doi.org/https://doi.org/10.1016/S1056-8719\(99\)00026-X](https://doi.org/https://doi.org/10.1016/S1056-8719(99)00026-X), 1999.
- Vecchi, G. and Soden, B.: Global Warming and the Weakening of the Tropical Circulation, *Journal of Climate - J CLIMATE*, 20, <https://doi.org/10.1175/JCLI4258.1>, 2007.
- Webb, P.: Introduction to Oceanography, Roger Williams University, <http://rwu.pressbooks.pub/webboceanography>, 2021.
- Yamaguchi, R. and Suga, T.: Trend and Variability in Global Upper-Ocean Stratification Since the 1960s, *Journal of Geophysical Research: 550 Oceans*, 124, 8933–8948, <https://doi.org/10.1029/2019JC015439>, 2019.
- Yang, H. and Wang, F.: Revisiting the Thermocline Depth in the Equatorial Pacific, *Journal of Climate*, 22, 3856–3863, <https://doi.org/10.1175/2009JCLI2836.1>, 2009.
- Yu, H., Tsuno, H., Hidaka, T., and Jiao, C.: Chemical and thermal stratification in lakes, *Limnology*, 11, 251–257, <https://doi.org/10.1007/s10201-010-0310-8>, 2010.
- 555 Zelle, H., Appeldoorn, G., Burgers, G., and van Oldenborgh, G. J.: The Relationship between Sea Surface Temperature and Thermocline Depth in the Eastern Equatorial Pacific, *Journal of Physical Oceanography*, 34, 643–655, <https://doi.org/10.1175/2523.1>, 2004.